

Relationship between occurrence of lahar and hydraulic properties of ashfall covered ground in the Arimura River basin of Sakurajima Volcano, Japan

Hayato Sugawara^{1*}, Yutaka Gonda²

¹Graduate School of Science and Technology, Niigata University, Niigata, JAPAN

²Faculty of Agriculture, Niigata University, Niigata, JAPAN

*Corresponding author: tyhrwgs@gmail.com

SUBMITTED 30 December 2024 REVISED 10 March 2025 ACCEPTED 10 March 2025

ABSTRACT When volcanic ash accumulates on the surface layer of slopes, it decreases the hydraulic conductivity of the ground, which can trigger lahars even due to small rainfall. Understanding the impact of changes in surface conditions on lahar occurrence is crucial for disaster prevention. This study employed a runoff analysis model based on the kinematic wave method to evaluate the surface conditions indirectly by hydraulic conductivity parameter values at the time of lahar occurrence. This study tried to reveal the relationship between the change of hydraulic conductivity parameter values in each lahar event and observed monthly ashfall data. The study area is the Arimura River basin in Sakurajima, Japan. Sakurajima volcano is still active today (2025), and new fresh volcanic ash is depositing on the surface ground. As a result, the model can find the optimal parameter in 41 out of 55 lahar events that occurred in the Arimura River basin on Sakurajima between 2015 and 2020. Next, we examined the characteristics of lahar events that could not be reproduced by our runoff analysis model. As a result, we found that lahars which occur after a lot of volcanic ashfall or contain large boulders have bad reproducibility. Next, we analyzed the relationship between the optimal parameter values for the 41 events and the monthly observed ashfall data. The results indicated a trend in which the optimal parameters decrease under conditions of increasing monthly ashfall, and the coefficient of determination was approximately 0.18. When considering the effect of preceding rainfall prior to lahar, a visual tendency was observed for the hydraulic conductivity parameter values to decrease with increasing preceding rainfall.

KEYWORDS Ashfall, Hydraulic Conductivity, Lahar, Runoff analysis, Kinematic wave model

© The Author(s) 2025. This article is distributed under a Creative Commons Attribution-ShareAlike 4.0 International license.

1 INTRODUCTION

In volcanic regions, volcanic ash ejected by volcanic activity accumulates on the ground surface. When volcanic ash accumulates on the ground, the infiltration capacity of the ground surface is significantly reduced, preventing rainfall infiltration (Jitousono and Shimokawa, 1989). Rainfall that fails to infiltrate the soil contributes to surface runoff, which travels downslope, entraining and eroding the unconsolidated volcanic ash deposits, ultimately resulting in the formation of a lahar (Oktariyanti et al., 2023). Thus, it is known that volcanic ash deposited on the ground surface has a strong influence on the generation of lahar in volcanic regions (Fukushima and Ishihara, 2006). To predict the timing and magnitude of lahars, it is important to clarify the relationship between changes in surface conditions caused by ash deposition, rainfall, and the generation of lahars.

The frequency and magnitude of lahars typically exhibit a temporal decline following the cessation of volcanic activity, coinciding with the termination of a consistent supply of freshly erupted volcanic ash (Gonda et al., 2014). The observed reduction in the frequency and magnitude of lahars is attributed to alterations in the surface environment, including the coarsening of

surface materials as a result of rainfall-induced erosion and the progressive reestablishment of vegetation cover. Teramoto et al. (2002) summarized dynamic observations of lahars at Mt. Unzen, Japan, from 1995 to 2000. They reported that the frequency, magnitude, and discharge rate of lahars gradually decreased after 1996. Additionally, the threshold for lahar initiation, represented by the maximum 10-minute rainfall, increased over time. These findings indicate a decreasing likelihood of lahar occurrence. Volcanic activity at Mt. Unzen ceased in February 1995. This marked the beginning of a period during which environmental conditions became progressively less conducive to lahar occurrence. Teramoto et al. (2002) suggested that this change occurred because fine-grained pyroclastic materials that had covered the surface were washed away by erosion. This made the surface course, improving rainfall infiltration and reducing the conditions for surface runoff. Yamakoshi and Suwa (1998) observed rainfall-induced surface runoff and sediment discharge on pyroclastic flow deposit slopes of Mt. Unzen from April 1996 to September 1997. They reported a significant decrease in sediment discharge and explained this as the result of rapid herbaceous vegetation growth following aerial seeding, which made the slopes less prone

to erosion. These findings are consistent with previous studies reporting that the frequency and magnitude of lahars tend to decline over time following the cessation of volcanic activity.

However, if volcanic activity resumes or new eruptions occur, leading to the accumulation of fresh volcanic ash on the ground, surface conditions may revert to a state more susceptible to lahar generation. Teramoto et al. (2005) conducted experiments at Sakurajima Volcano in Japan, assuming two phases: an active volcanic phase and a quiet phase. They prepared two slopes with volcanic ash applied to the surface and slopes without ash and observed rainfall and sediment runoff on each slope. The results showed that surface and sediment runoff increased on the slopes after volcanic ash application, indicating a shift to surface conditions more favorable for lahar occurrence. Evaluating the risk, frequency, and magnitude of lahars can be effectively achieved by measuring hydraulic conductivity in upstream areas proximal to the crater, where rainfall and sediment discharge are most likely to originate (Kinoshita et al., 2013). However, access to crater-adjacent areas is often restricted due to safety concerns, making it difficult to measure hydraulic conductivity directly. Moreover, in active volcanoes like Sakurajima and Aso in Japan, new volcanic ash is frequently deposited over short intervals. As a result, conducting basin-wide field measurements after each eruption requires considerable effort.

Our research group has proposed a method to indirectly assess surface conditions on a watershed scale during lahar events by performing inverse analysis using a rainfall-runoff simulation model. Teramoto et al. (2003) demonstrated that the runoff process of lahars in volcanic regions can be largely reproduced using the Kinematic wave method. Building on this study, we developed a runoff model based on the Kinematic wave method to evaluate the surface condition indirectly by reproducing the actual measured hydrographs (Ersöz et al., 2023, 2024). The core aspect of this evaluation method lies in its ability to reproduce the hydrograph waveforms of lahars accurately. Initially, we used a runoff coefficient as the calculation parameter to represent surface conditions during lahar events. Our model assumed that a constant proportion of rainfall, represented by a runoff coefficient, is converted to runoff (Ersöz et al., 2023). To assess the model's performance, we conducted runoff analyses for 62 lahar events that occurred in the Arimura River basin at Sakurajima, Japan, between 2015 and 2020. However, for more than half of the events, the observed hydrograph waveforms could not be reproduced, making it difficult to evaluate the surface conditions. We identified the primary issue as the assumption that a constant proportion of rainfall is converted to runoff. To improve the reproducibility of the runoff model, we revised our assumptions: rainfall exceeding the hydraulic

conductivity of the surface becomes surface runoff, and the hydraulic conductivity of the surface varies depending on the amount of volcanic ash deposits. Subsequently, we adopted hydraulic conductivity as the parameter representing surface conditions in our runoff analyses. This adjustment improved the accuracy of hydrograph reproduction, but about 40% of the lahar events were not well reproduced (Ersöz et al., 2024).

In this study, to enable the evaluation of hydraulic conductivity during more lahar events and analyze relationship between the hydraulic conductivity and volcanic ash deposition, we revise the criteria used to assess the reproducibility of the hydrographs. In our previous study (Ersöz et al., 2024), we assessed the reproducibility of the hydrograph waveform by judging the overall waveform, peak flow rate, and the timing of the start/end of the waveform. However, we argue that, for evaluating lahar hazards, reproducing the peak flow is more critical than other elements. Therefore, this study focuses on whether the observed peak flow was accurately reproduced and revises the criteria for assessing reproducibility. Additionally, upon reviewing the rainfall and water level data for the 62 lahar events that occurred between 2015 and 2020, we identified missing or incomplete data in several events. Consequently, these events were excluded from the analysis, reducing the total number of target events to 55. We then re-analyzed these lahars following the same procedures. Afterwards, we classified the events based on whether the hydrographs were accurately reproduced as in Ersöz et al. (2024). For the events with poor reproducibility, we investigated the causes of the discrepancies. In contrast, for those with good reproducibility, we aimed to reveal the relationship between the evaluated hydraulic conductivity and the observed ashfall data for each event.

2 STUDY AREA

The study area is the Arimura River basin in Sakurajima, Kagoshima Prefecture (Figure 1). Sakurajima is an active volcano with ongoing volcanic activity, where the emission of volcanic ash and other materials continuously alters the surface conditions. In this study, the research area is defined as a 2.8 km² region, with the First Arimura Bridge, located approximately 2.5 km south-southeast of the Minamidake crater, as the downstream boundary. To monitor lahar in this basin, wire sensors, ultrasonic water level gauges, and flow velocity meters have been installed by the Osumi River National Road Office and the Ministry of Land, Infrastructure, Transport and Tourism (MLIT) Japan. In the Arimura River basin, 3 wire sensors are installed at the water-through part of the Sabo dam in a 60 cm interval, and the occurrence and scale of lahar are determined by the cutting of the wires (Itoh et al., 2025). The wire sensors are located 600 m downstream of the Arimura

No.3 Sabo dam (Tetsuka et al., 2021). Over the past 10 years, from 2013 to 2023, an average of 9.6 lahars per year have been observed. Additionally, ashfall measurements are conducted near the First Arimura Bridge. In this study, two types of volcanic ash observation data were used: daily observation data and monthly observation data. The daily observation data were collected at the Kagoshima Prefectural Meteorological Observatory, located 20 km southwest of the Minamidake crater (red point in Figure 1). The monthly observation data were collected approximately 2 km south of the Minamidake crater (blue point in Figure 1).

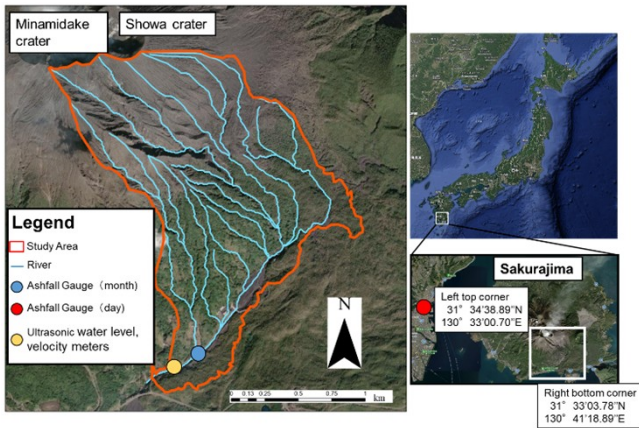


Figure 1 Location of the basin and equipments.

3 METHODOLOGY

3.1 Kinematic Wave Model

In this study, we employed a runoff analysis model based on the kinematic wave method, dividing the study area into 24 sub-basins for the analysis (Ersöz et al., 2024) (Figure 2). Each sub-catchment consists of a channel and slopes on both sides of it, and discharge is calculated individually. The discharge calculated in each sub-catchment is added up, starting from upstream, and finally, the discharge at the most downstream point is treated as the calculated discharge from the drainage area. It is assumed that the discharge calculated in the upstream is not restricted by the downstream conditions (Ministry of Agriculture, Forestry and Fisheries, 2019).

Each slope is modeled as consisting of two layers: a volcanic ash layer and a soil layer (Figure 3). Each layer has a designated hydraulic conductivity parameter value. These express the saturated hydraulic conductivity, and the surface runoff is determined according to the hydraulic conductivity value, which is set as a parameter and the rainfall intensity. When rainfall intensity is smaller than the hydraulic conductivity, all the rainfall infiltrates into the soil layer. When rainfall intensity exceeds the hydraulic conductivity of the volcanic ash layer, water infiltrates into the volcanic ash

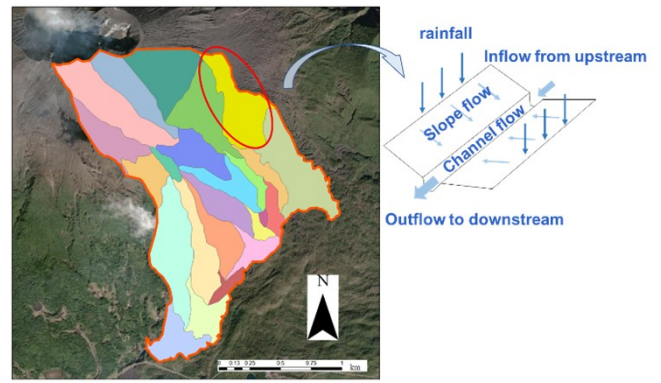


Figure 2 Modeling of each sub-catchment.

layer according to the parameter values, and the rest of the water is calculated as surface runoff. Water that infiltrates the volcanic ash layer continues to infiltrate into the soil layer according to the soil layer’s hydraulic conductivity parameter value, while the remainder is treated as interflow within the volcanic ash layer. The thickness of the volcanic ash layer is set to 16 cm (Teramoto et al., 2005), and porosity is set to 0.5 (Miyata and Fujita, 2013).

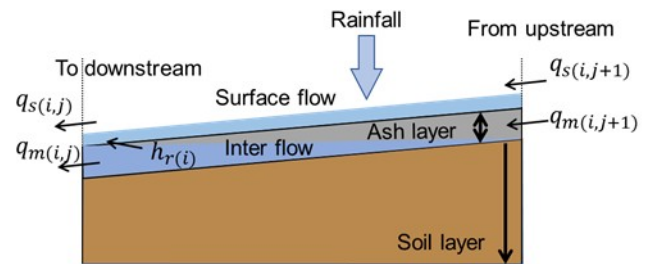


Figure 3 Schematic diagram of slope flow calculation.

Surface, intermediate, and channel flows were obtained by solving the continuity equations and equations of motion numerically. The continuity equations and equations of motion for slope flow are Equations (1) and (2), for intermediate flow are Equations (4) and (5), and for channel flow are Equations (6) and (7). The Manning law is used for the equations of motion for the surface and channel flows, and the Darcy law for the intermediate flow. Constants K in Equation (2), (5), and (8) are obtained from Equation (3), (6), and (9), respectively, and the slope and channel flow constants p are 3/5 and the constant p in the intermediate flow is 1 (Sugiyama, 1980).

Slope flow:

$$\frac{\partial h_s}{\partial t} + \frac{\partial q_x}{\partial x} = r - f_1 \tag{1}$$

$$h_s = K q_s^p \tag{2}$$

$$K = n_s^{\frac{3}{5}} S_s^{-\frac{3}{10}} \tag{3}$$

Intermediate flow:

$$\frac{\partial h_m}{\partial t} + \frac{\partial q_m}{\partial x} = f_1 - f_2 \quad (4)$$

$$h_m = K q_m^p \quad (5)$$

$$K = \frac{\lambda}{k S_s} \quad (6)$$

Channel flow:

$$\frac{A}{\partial t} + \frac{Q}{\partial x} = q_s \quad (7)$$

$$A = K q_s^p \quad (8)$$

$$K = n_c^{\frac{3}{5}} S_c^{-\frac{3}{10}} \quad (9)$$

where h_s is surface flow height (m), q_s is surface flow discharge rate (m^2/s) per unit width, t is time step (s), x is distance (m), r is rainfall intensity (m/s), f_1 is infiltrated water velocity in volcanic ash (m/s), K and p are model constants, n_s is denoted for Manning's roughness coefficient for slope ($\text{m}^{-1/3}/\text{s}$), S_s is slope gradient for slope, h_m is intermediate water height (m), q_m is intermediate flow discharge (m^3/s), λ is porosity (0.5), k is saturated hydraulic conductivity, f_2 is infiltrated water velocity into soil layer (m/s), n_c is denoted for Manning's roughness coefficient for channel ($\text{m}^{-1/3}$ s), S_c is slope gradient for channel, A is river channel cross-section area (m^2) and Q is channel discharge (m^3/s).

In this study, equations (1), (2) for slope flow, (4), (5) for intermediate flow, and (7), (8) for channel flow were rewritten into the following difference equations.

Slope flow:

$$h_{s(i+1,j)} = h_{s(i,j)} - \frac{\Delta t}{\Delta x} (q_{s(i,j)} - q_{s(i,j+1)}) + \Delta t (r_{(i)} - f_1) + h_{r(i)} \quad (10)$$

$$q_{s(i,j)} = \frac{1}{n_c} h_{s(i,j)}^{\frac{5}{3}} S_s^{\frac{1}{2}} \quad (11)$$

Intermediate flow:

$$h_{m(i+1,j)} = h_{m(i,j)} - \frac{\Delta t}{\Delta x} (q_{m(i,j)} - q_{m(i,j+1)}) + \frac{\Delta t}{\lambda} (f_1 - f_2) + \frac{1}{\lambda} h_{r(i)} \quad (12)$$

$$q_{m(i,j)} = h_{m(i,j)} S_s k \quad (13)$$

Channel flow:

$$A_{(i+1,j)} = A_{(i,j)} - \frac{\Delta t}{l} (Q_{(i,j)} - Q_{(i,j+1)}) + \Delta t q_{s(i)} \quad (14)$$

$$q_{(i,j)} = \frac{1}{n_c} A_{(i,j)} R^{\frac{2}{3}} S_c^{\frac{1}{2}} \quad (15)$$

where h_r is an increment of water depth due to return flow (m), R is the hydraulic radius (m), l is the length between adjacent cross sections (m), i is the time step number (s), and j is the cross-section number. Δt is 0.1 s, Δx is 20 m. n_c is set to 0.03 based on the list of approximate values of roughness coefficients (Japan Society of Civil Engineers, 1999).

Ersöz et al. (2024) assumed that no runoff occurs from the vegetated area in the middle and lower basin of the Arimura River, and that most of the rainfall runoff occurs from the upstream barren area. They set the hydraulic conductivity of the vegetated area at a constant value of 90 mm/hr and only changed the parameter values of hydraulic conductivity and equivalent roughness in the upstream barren area to match waveforms of calculated hydrographs and observed hydrographs. To simplify the calculations in this study, we applied the same parameters across the entire watershed. For all other conditions, we followed the same methodology as in the study by Ersöz et al. (2024).

This calculation is performed for the slopes in each sub-catchment, and surface runoff and interflow accumulated at the base of the slopes are combined to form channel flow. By adding the channel flow for each sub-catchment sequentially from upstream, the total runoff from the drainage area is calculated at the downstream end of the watershed.

3.2 Overview of Runoff Analysis

Here, we calculated 55 lahar events that occurred between 2015 and 2020 using a model based on the Kinematic Wave method, aiming to identify optimal parameters that could reproduce the peak flow of the observed runoff waveforms. In this study, two parameters were used to represent the surface conditions: hydraulic conductivity and equivalent roughness.

We conducted hydraulic conductivity tests using a mini-disk infiltrometer (Meter, USA) based on the mini-disk infiltrometer user manual (METER Group, Inc., 2021) in the lower reaches of the Sakurajima Arimura River from 2022 to 2023 (Table 1, Figure 4). In this study, we set up the range of hydraulic conductivity parameter values, referring to the results of the mini-disk infiltrometer, from 0 mm/hr to 50 mm/hr and varied by 5 mm/hr. For the equivalent roughness, assuming a realistic range of values, we set up the range from 0.05 to 1.00 and varied by 0.05 increments (Japan Society of Civil Engineers, 1999). Adjusting the values of

these parameters changes the calculated runoff hydrograph. Among the numerous combinations of parameter values, those that most accurately reproduced the observed runoff hydrograph were identified as the optimal parameters (Figure 5). After completing the runoff analysis for all 55 lahar events, the events were classified into those where the waveforms were well reproduced and those where they were not. For the events with poor results, we investigated the reasons for the poor waveform reproduction. For the events with good reproduction results, we analyzed the relationship between observed ashfall data and optimal parameter values.

Table 1. The time and values of the mini-disk infiltrometer

	Location							
	1	2	3	4	5	6	7	8
Time	Nov, 2022				Oct, 2023			
HC value (mm/hr)	35.5	22.1	12.3	28.4	38.6	35.5	15.0	23.0

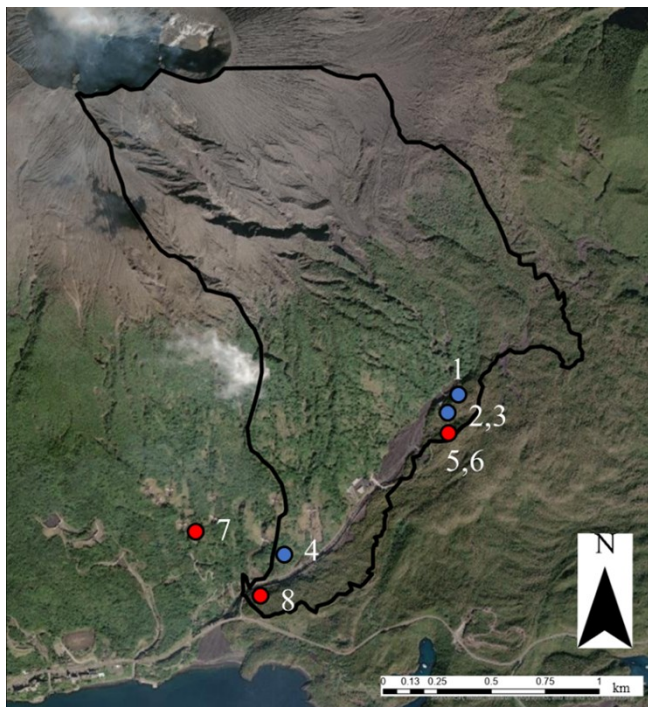


Figure 4 Exact point of mini-disk infiltrometer test.

In this study, we updated the criteria used to assess the reproducibility of the events. The criteria are as follows (Figure 6):

- The model accurately reproduces the peak flow of the observed hydrograph without any time lag.
- No unnatural discharge is calculated when no actual runoff occurs.

Ersöz et al. (2024) judged the reproducibility based on the criteria listed below:

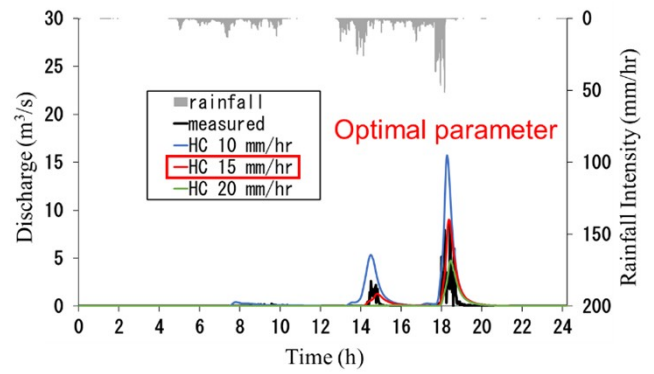


Figure 5 Example of seeking optimal parameters.

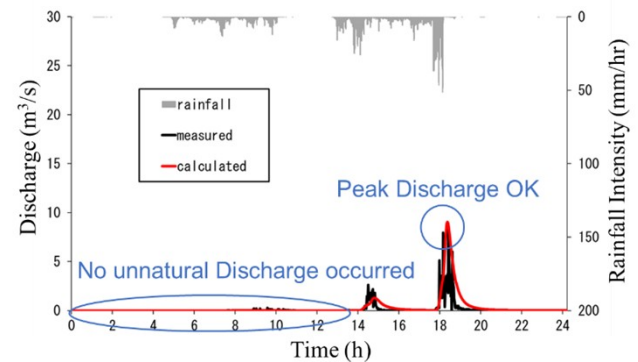


Figure 6 New criteria in this study.

- The waveform of measured data and the hydrograph calculated by the kinematic wave model should be matched.
- The event start/end moment of the measured data and the hydrograph calculated by the kinematic wave model should be matched.
- Peak discharge value of measured data and the hydrograph calculated by the kinematic wave model should be matched.

In this study, we considered the reproducibility of the peak flow rate to be most important and judged the reproducibility to be good if the model reproduced the peak of the measured discharge and no unnatural runoff was observed in other parts of the model.

3.3 Data Used for Runoff Analysis

For runoff analysis, topographic data of the basin, rainfall data, and observed discharge data used for waveform comparison were required. The topographic data was obtained by downloading a 5-meter mesh Digital Elevation Model (DEM) from the Geospatial Information Authority of Japan's Fundamental Geospatial Data download service (<https://fgd.gsi.go.jp/download/mapGis.php?tab=dem>) and was processed using ArcGIS. Rainfall data were downloaded from the XRAIN Real-Time Rainfall Display and Download System of

the Data Integration and Analysis System (DIAS) (<http://apps.diasjp.net/xband/>) and utilized for the analysis. The XRAIN data has a temporal resolution of 1 minute and a spatial resolution of 250-meter mesh. The observed discharge data for each lahar event were calculated using water level and flow velocity data near the First Arimura Bridge.

The observed discharge data for each lahar was calculated from water level data of the ultrasonic water level gauge near the First Arimura Bridge by using Manning's law, shown in Equation (16), (17).

$$v = \frac{1}{N} R^{\frac{2}{3}} S^{\frac{1}{2}} \quad (16)$$

$$Q = Av \quad (17)$$

where v is flow velocity (m/s), N is the Manning roughness coefficient, R is hydraulic radius (m), S is the gradient of the channel, Q is discharge (m³/s), A is cross-sectional area of the flow (m²). The gradient of channel S and roughness coefficient N were taken from the observation record of Takahashi et al. (2017), $S = 1/15.5$, $N = 0.01$. A was obtained by multiplying the observed water level h by the river width of 15 m.

4 RESULTS

4.1 Reproducibility of the Hydrograph

Among the 55 lahar events analyzed, 41 events successfully reproduced the observed waveforms well (Figure 7a). However, for the remaining 14 events, the waveforms could not be reproduced (Figure 7b). Using the evaluation criteria used in Ersöz et al. (2024), the hydrograph reproducibility was approximately 54%. In contrast, when applying the criteria in this study, the hydrograph reproducibility increased to approximately 74%. It was confirmed that the optimal hydraulic conductivity values are slightly larger than those of Ersöz et al. (2024) because we set up a constant hydraulic conductivity value for the entire watershed. However, the coefficients of determination for both are highly correlated at more than 0.8 (Figure 8). In this study, lahars with good waveform reproducibility are referred to as "regular lahars", while those with poor waveform reproducibility are referred to as "irregular lahars". In the next section, we discuss the characteristics of irregular lahars.

4.2 Characteristics of Irregular Lahar

First, we analyzed the 14 irregular lahar events by comparing the observed discharge waveforms with those calculated by the model and classified them into 4 types based on shared characteristics (Table 2; Figure 9a-d).

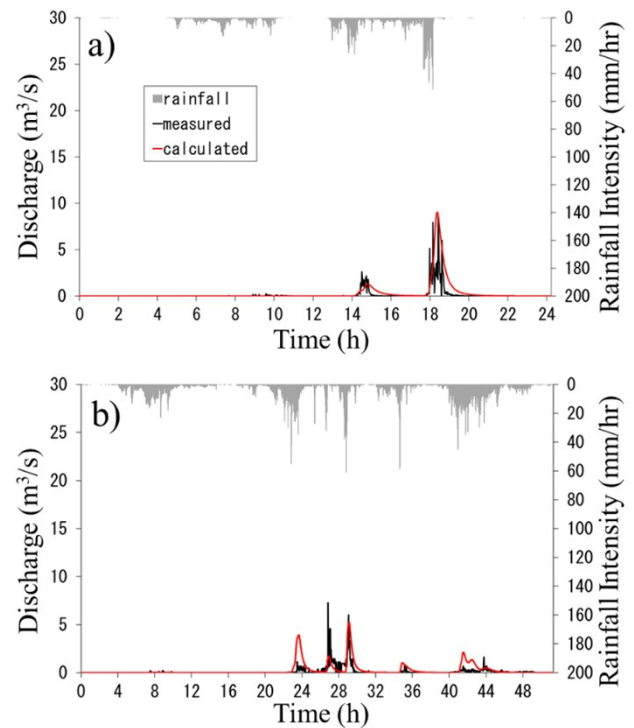


Figure 7 Example of waveforms for regular and irregular lahar.

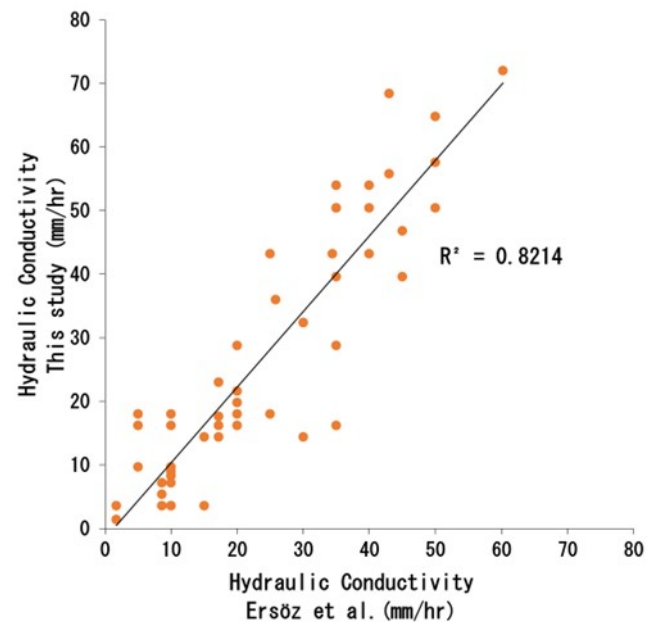


Figure 8 Optimal hydraulic conductivity parameter value in each study.

Among the 4 types of lahar events, it was found that for Types 1 and 2, events, while the calculated flow may be slightly overestimated in either the early or later part, the overall waveform shape can be reproduced by adjusting the hydraulic conductivity parameter values. In contrast, for Types 3 and 4, matching the peak flow by adjusting the hydraulic conductivity parameter values resulted in a significant overestimation of runoff in the non-peak part. Therefore, it was impossible to identify

Table 2. Characteristics of each lahar type

Type	Characteristics	Number
1 (Figure 9a)	Difficult to reproduce the early part of the observed runoff waveform	4
2 (Figure 9b)	Difficult to reproduce the early part of the observed runoff waveform	2
3 (Figure 9c)	Having an outstanding peak runoff waveform	4
4 (Figure 9d)	Having a longer duration of runoff	4

appropriate parameter values for these events. In Section 5.1, we will focus on the lahar events of Type 3 and 4, by examining their runoff features in detail.

5 DISCUSSION

5.1 Runoff Properties of Irregular Lahars

First, we examined the runoff ratio for each event by dividing the total effective rainfall by the total rainfall (Figure 10). Figure 10 shows that lahars classified as Type 3 and Type 4 exhibit higher runoff ratios compared to those of other types of lahars.

Next, we analyzed the relationship between daily ashfall observation data from 2015 to 2020 and the occurrence of Type 3 and Type 4 lahars (Figure 11). The Type 1 and 2 event groups are not shown in the graph because no relationship with ashfall could be found. The daily ashfall data were obtained from the Kagoshima Local Meteorological Observatory, located 20 km southwest of the Showa crater in Sakurajima, as mentioned in Chapter 2. Technically, the ashfall distribution around the Arimura River may differ from the place of Kagoshima Prefectural Meteorological Observatory; however, it was considered that this discrepancy would not significantly affect the analysis of the relationship between daily ashfall variations and lahar occurrence. Therefore, the data were used as-is for the analysis. Figure 11 reveals a clear trend: Type 4 lahars tend to occur after significant ashfall events, where ash accumulation exceeds 50 g/m².

From these results, we estimate that Type 4 lahars tend to occur when large amounts of volcanic ash accumulate on the surface, reducing the ground's infiltration capacity. Additionally, due to the heavy accumulation of volcanic ash, Type 4 lahars likely contain a higher concentration of volcanic ash compared to other types. The runoff analysis conducted in this study, which employs the Kinematic Wave method, calculates runoff under the assumption that lahar flow is equivalent to clear water flow in the calculation. There-

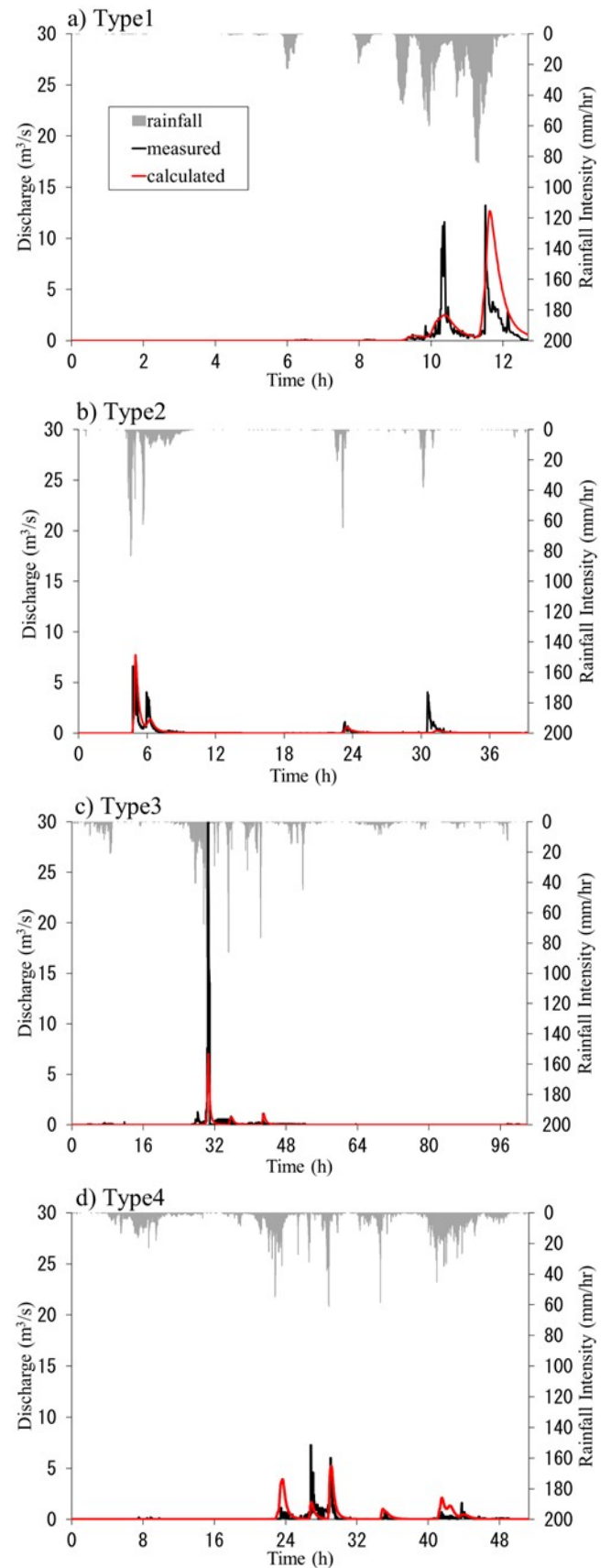


Figure 9 Example of waveforms for each lahar type.

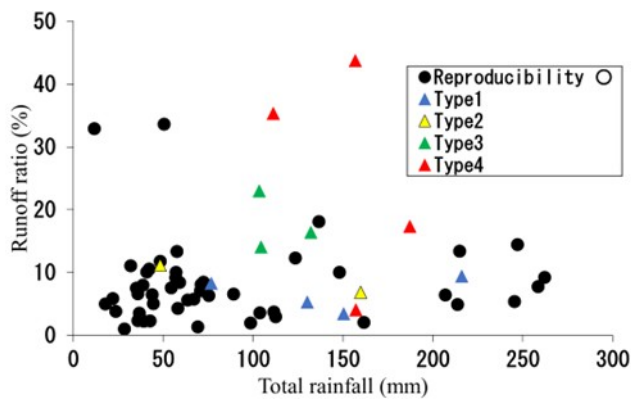


Figure 10 Total rainfall and runoff ratios for each lahar type.

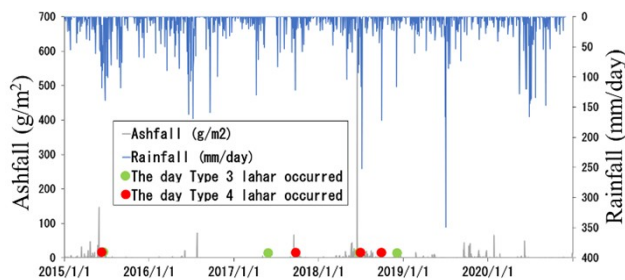


Figure 11 Total rainfall and runoff ratios for each lahar type.

fore, lahars with a high concentration of sediment or volcanic ash are less likely to be accurately reproduced by the model's waveform.

For Type 3 lahars, like Type 4, they occur when the runoff ratio is higher compared to other types of lahars. However, as shown in Figure 11, no significant ashfall was observed in the days just before the lahar events. Therefore, we checked the water level data for these events and found that the water level didn't increase gradually but increased and decreased rapidly in 1 minute. Currently, ultrasonic water level gauges are used to monitor lahar water levels. These gauges measure water levels based on the reflection of ultrasonic waves; however, they cannot distinguish between water and rocks within the lahar. Therefore, we assume the sudden peak in Type 3 lahars is likely not an extremely high peak flow. It appears that a large boulder is present at the point where the ultrasonic waves were reflected, leading to the sudden high-water level. These Type 3 event groups were considered outliers and excluded from the analysis.

5.2 Relationship Between Optimal Hydraulic Conductivity in Regular Events and Ashfall

Focusing on 41 regular lahar events, we analyzed the relationship between the optimal hydraulic conductivity parameter for each event and monthly ashfall data (Figure 12). As a result, we found that the hydraulic conductivity tends to be high when the amount of ash-

fall is low and decreases as the amount of ashfall increases. However, the coefficient of determination for the logarithmic regression of the relationship was low at 0.1795, indicating that there is no clear relationship between these. When the monthly ashfall is 0 cm to 0.1 cm, the hydraulic conductivity values vary widely from 5 mm/hr to 50 mm/hr. The reason for the low coefficient of determination is due to the wide range of hydraulic conductivity values

We considered that one reason for the scatter in hydraulic conductivity values may be the effect of preceding rainfall. If there is a large amount of preceding rainfall before the lahar, the volcanic ash on the surface layer will be washed away, and the hydraulic conductivity of the ground surface will be high. In contrast, if the amount of preceding rainfall prior to the event is small, the volcanic ash may remain on the surface layer, or crust might be generated due to chemical cohesion by combing with small amounts of rainfall and volcanic ash and the hydraulic conductivity of the ground surface will be low (Onda et al., 1996). We considered that such a process occurred in Sakurajima, and it caused the variation in the hydraulic conductivity values.

Therefore, we calculated the amount of preceding rainfall from 7 days before to the day of the lahar and color-coded the scatter plot in Figure 12 based on the amount of preceding rainfall (Figure 13). The results indicated a trend where lower values of hydraulic conductivity corresponded to less preceding rainfall, while higher preceding rainfall amounts were associated with increased hydraulic conductivity values.

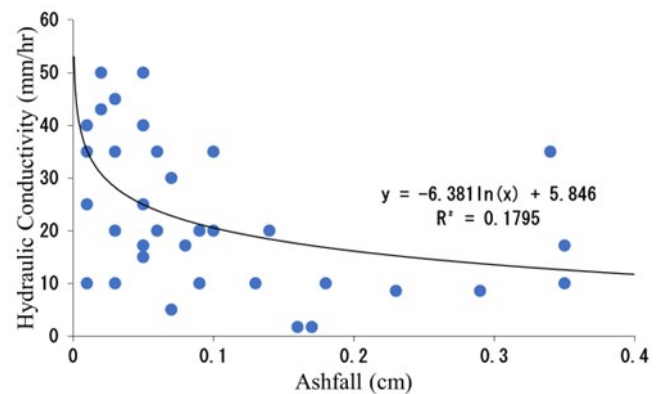


Figure 12 Total rainfall and runoff ratios for each lahar type.

We believe that one of the reasons why hydraulic conductivity increases when there is a lot of preceding rainfall is that the fine-grained volcanic ash deposited on the surface layer flows out with the rainfall. Ogawa et al. (2003) conducted an experiment to understand the behavior of rainfall runoff on a slope where volcanic ash was spread on the ground surface and reported that fine-grained volcanic ash (0.42 mm or less) deposited on the ground surface easily moved with very little sur-

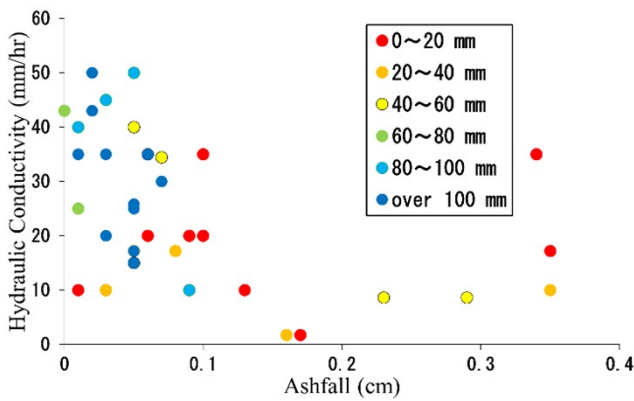


Figure 13 Total rainfall and runoff ratios for each lahar type.

face runoff. Considering the results of this report and Figure 13 simultaneously, it can be considered that the fine-grained volcanic ash deposited on the surface layer of the ground is washed away by a large amount of rainfall, and the ground becomes coarser-grained, resulting in a higher hydraulic conductivity. In addition, the active crater at Sakurajima has changed from the Showa crater to the Minamidake crater after 2018. The results of studies by Kozono et al. (2019) and Freret-Lorgeril et al. (2022) suggest that the grain size of volcanic ash ejected from the Minamidake crater has a finer component than that of the Showa crater. In this study, the relationship between the optimal parameter values and observed ashfall data for each lahar event was analyzed together from 2015 to 2020, but the runoff characteristics of lahar may change depending on the differences in the grain size of the volcanic ash deposited on the ground surface. This part will be the subject of future research.

6 CONCLUSION

The aim of the study was to evaluate hydraulic conductivity during the lahar events by using the runoff analysis model and clarify the relationship between hydraulic conductivity and the observed ashfall data. To increase the available hydraulic conductivity data during lahar events for the analysis, the criteria for assessing hydrograph reproductivity from a previous study were revised, focusing on the accurate reproduction of peak flow rather than other elements. The study re-examined 55 out of 62 lahars that occurred in Sakurajima between 2015 and 2020, excluding incomplete data. The results showed that the model successfully reproduced waveforms for 41 lahar events and identified characteristics of 14 irregular lahar events. An analysis of the 41 regular lahars and the monthly ashfall observations revealed a general trend of decreasing hydraulic conductivity values with increasing ashfall, with their coefficient of determination being approximately 0.18. Next, we analyzed the relationship between the amounts of preceding rainfall from seven

days prior to the lahar events and hydraulic conductivity parameter values. When the hydraulic conductivity parameter values are less than 0.1 cm, they are scattered, but we found the possibility that the hydraulic conductivity tends to be larger when the preceding rainfall is high and smaller when the preceding rainfall is low. The goal of this study is to predict the on-site hydraulic conductivity based on the observed ashfall, rainfall, and the actual lahar water level data. In the future, it is necessary to analyze in more detail the relationship between the thickness of the remaining volcanic ash deposits on the ground surface or the amount of preceding rainfall, and the hydraulic conductivity

DISCLAIMER

The authors declare no conflict of interest.

ACKNOWLEDGMENTS

We would like to thank Osumi River National Road Office, and Ministry of Land, Infrastructure, Transport and Tourism (MLIT) Japan who provided valuable support in this study.

REFERENCES

- Ersöz, T., Haneda, K. and Gonda, Y. (2024), 'The role of volcanic ash thickness on the hydraulic conductivity of the ground and the initiation of debris flows', *Natural Hazards* **120**, 10969–11007.
 URL: <https://doi.org/10.1007/s11069-024-06654-6>
- Ersöz, T., Haneda, K., Kuribayashi, A. and Gonda, Y. (2023), 'Temporal changes in lahar sediment run-off characteristics and run-off coefficients in the arimura river basin of sakurajima volcano, japan', *Earth Surface Processes and Landforms* **48**(14), 2682–2703.
 URL: <https://doi.org/10.1002/esp.5654>
- Freret-Lorgeril, V., Bonadonna, C., Rossi, E., Poulidis, A. P. and Iguchi, M. (2022), 'New insights into real-time detection of tephra grainsize, settling velocity and sedimentation rate', *Scientific Reports* **12**(4650).
 URL: <https://doi.org/10.1038/s41598-022-08711-1>
- Fukushima, M. and Ishihara, K. (2006), 'Debris flows at sakurajima: its relationship with rainfall and volcanic activity', *Annuals, Disaster Prevention Research Institute, Kyoto University* **49B**, 355–362.
- Gonda, Y., Legono, D., Sukatja, B. and Santosa, U. B. (2014), 'Debris flows and flash floods in the putih river after the 2010 eruption of mt. merapi, indonesia', *International Journal of Erosion Control Engineering* **7**(2), 63–68.
 URL: <https://doi.org/10.13101/ijece.7.63>

Itoh, T., Tagata, S. and Mizuyama, T. (2025), 'Debris flow detection by combinations of lvp sensors and wires: Examples in sakura-jima island, japan', *Journal of the Civil Engineering Forum* **11**(1), 23–32.

URL: <https://doi.org/10.22146/jcef.13869>

Japan Society of Civil Engineers (1999), *水理公式集*, Tokyo: Maruzen.

Jitousono, T. and Shimokawa, E. (1989), 'Surface runoff on tephra-covered hillslope in sakurajima volcano', *Journal of Japan Society of Erosion Engineering, Shin-Sabo* **42**(3), 18–23.

URL: https://doi.org/10.11475/sabo1973.42.3_18

Kinoshita, A., Sakai, Y., Ohno, R., Sato, A. and Nishikubo, F. (2013), 'Vegetation and soil properties of sakurajima volcanic ash and their effect on the in situ infiltration rate of surface soil', *Journal of Japan Society of Erosion Engineering* **65**(6), 30–36.

URL: https://doi.org/10.11475/sabo.65.6_30

Kozono, T., Iguchi, M., Miwa, T., Maki, M., Maesaka, T. and Miki, D. (2019), 'Characteristics of tephra fall from eruptions at sakurajima volcano, revealed by optical disdrometer measurements', *Bulletin of Volcanology* **81**(41).

URL: <https://doi.org/10.1007/s00445-019-1300-2>

METER Group, Inc. (2021), 'Mini disk infiltrometer manual'. Accessed 7 March 2025.

URL: https://www.labcell.com/media/24285/20421_mini_disk_manual_web.pdf

Ministry of Agriculture, Forestry and Fisheries (2019), '土地改良事業計画設計基準及び運用・解説「排水」'. Accessed 7 March 2025.

URL: https://www.maff.go.jp/j/nousin/noukan/tyotei/ki_zyun/pdf/20200303130206/00_haisui_zentaiban.pdf

Miyata, S. and Fujita, M. (2013), 'Application of x-band radar and runoff model to debris flow frequency occurred creeks in sakurajima island', *Annuals, Disaster Prevention Research Institute, Kyoto University* **56B**, 457–464.

Ogawa, Y., Shimizu, A., Shimizu, T. and Miyabuchi, Y. (2003), 'An experimental study on surface runoff and sediment discharge on a slope covered with fine-grained volcanic ash', *Journal of Japan Society of Erosion Engineering* **55**(5), 22–30.

URL: https://doi.org/10.11475/sabo1973.55.5_22

Oktariyanti, S., Hidayah, E., Saifurridza, Ma' ruf, M. F., Hayati, N. N. and Yusop, Z. (2023), 'Mapping of mount semeru volcanic mudflow susceptibility along

the rejali river using the gis-based ahp-topsis ensemble approach', *Journal of the Civil Engineering Forum* **9**(3), 303–314.

URL: <https://doi.org/10.22146/jcef.6691>

Onda, Y., Takenaka, C. and Mizuyama, T. (1996), 'The mechanism inducing the infiltration rate lowering of unzen volcanic ash', *Journal of Japan Society of Erosion Engineering* **49**(1), 25–30.

URL: <https://doi.org/10.11475/sabo1973.49.25>

Sugiyama, H. (1980), 'An experimental study on the resistance law of rain water flow over on a slope surface', *Transactions of the Agricultural Engineering Society, Japan* **1980**(87), 16–23.

URL: https://doi.org/10.11408/jsidre1965.1980.87_16

Takahashi, Y., Mizuno, H., Fujimura, N., Yokoo, K., Ikeda, M. and Komuro, C. (2017), '桜島有村川での観測で得られた土石流表面形状による土石流の水量評価', *JSECE Publication* **81**, 766–767.

Teramoto, Y., Jitousono, T., Shimokawa, E. and Koga, S. (2002), 'Temporal variation of rainfall induced debris flows and their runoff characteristics in unzen volcano', *Journal of Japan Society of Erosion Engineering* **54**(5), 50–54.

URL: https://doi.org/10.11475/sabo1973.54.5_50

Teramoto, Y., Shimokawa, E. and Jitousono, T. (2003), 'The temporal variations of runoff processes of the debris flows at the mizunashi river in unzen volcano', *Journal of Japan Society of Erosion Engineering* **56**(3), 3–11.

URL: https://doi.org/10.11475/sabo1973.56.3_3

Teramoto, Y., Shimokawa, E. and Jitousono, T. (2005), 'Temporal change in the amount of rainwater and sediment discharge caused by ebb and flow of volcanic activity on mt. sakurajima', *Research bulletin of the Kagoshima University forests* **32**, 17–22.

Tetsuka, S., Hayashi, S. and Ishii, Y. (2021), 'Changes in slope erosion and sedimentation rates and its relations with the amount of ash fall and debris flow occurrence based on lidar data from 2010 to 2018 in the arimura river basin of sakurajima volcano, japan', *Journal of Japan Society of Erosion Engineering* **74**(4), 32–41.

URL: https://doi.org/10.11475/sabo.74.4_32

Yamakoshi, T. and Suwa, H. (1998), 'Responses of surface runoff and sediment discharge to revegetation on the slope of pyroclastic-flow deposits, mount unzen, japan', *Journal of Japan Society of Erosion Engineering* **51**(3), 3–10.

URL: https://doi.org/10.11475/sabo1973.51.3_3